BL-6C/2019G635

Valence-selective structural study on an Fe_3O_4 magnetite crystal by x-ray fluorescence holography

Shinya HOSOKAWA[1,*], Naohisa HAPPO[2], Artoni Kevin Roquero ANG[3], Koji KIMURA[3], and Kouichi HAYASHI[3]

[1] Institute of Industrial Nanomaterials, Kumamoto University, Kumamoto 860-8555, Japan
[2] Graduate School of Information Sciences, Hiroshima City University, Hiroshima 731-3194, Japan
[3] Department of Physical Science and Engineering, Nagoya Institute of Technology, Nagoya 466-8555, Japan

1 Introduction

One of the topics in structural studies of materials is the progress of x-ray fluorescence holography (XFH) technique with valence-selective properties. This becomes possible by employing the incident x-ray energy at a special one near an absorption edge and characteristic to a valency. For example, we have recently clarified the differences in the local atomic structures around the Yb^{2+} and Yb^{3+} ions in $YbInCu_4$ valence transition material three-dimensionally by this method [1].

Magnetite Fe_3O_4 is a typical mixed valence material with a coexistence of divalent Fe^{2+} and trivalent Fe^{3+} ions. Figure 1 shows the crystal structure of Fe_3O_4 obtained from x-ray diffraction, having a *fcc* structure with a space group of $Fd\bar{3}m$ and a lattice constant of 0.83153 nm in the standardized form [2], which is taken from Ref. [3]. Around Fe atoms, tetrahedral A sites and octahedral B sites coexist in the crystal, and the fractions of the A and B sites are 1/3 and 2/3 in the crystal, respectively. It is believed that a half of Fe^{3+} ions occupy the A sites, and the remaining half of the Fe^{3+} ions and all of the Fe^{2+} ions enter the B sites.

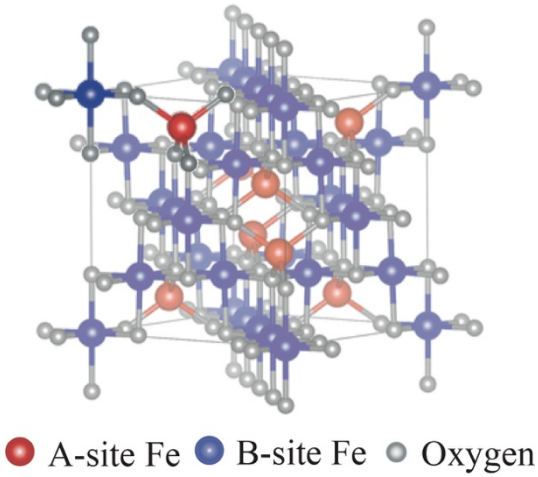

Fig. 1: Crystal structure of magnetite Fe_3O_4. After Ref. [3].

Since the ionic radii of Fe^{2+} and Fe^{3+} ions are different, i.e., 0.076 and 0.065 nm, respectively [4], the actual atomic positions of the neighboring atoms around these Fe ions would be different from each other. In this proposal, we tried to distinguish the local atomic structures by using the above valence-selective XFH technique.

2 Experiment

Figure 2 exhibits Fe *K* x-ray absorption near-edge structure (XANES) spectra of Fe_3O_4, FeO, and Fe_2O_3 indicated by the solid, dotted, and dashed curves, respectively, which is taken from Ref. [3]. An energy shift is observed in the absorption edges between the divalent FeO and the trivalent Fe_2O_3 by about 3 eV. In addition, a pre-edge is seen at about 7.114 keV for Fe_2O_3 and Fe_3O_4 originating from the Fe^{3+} ions.

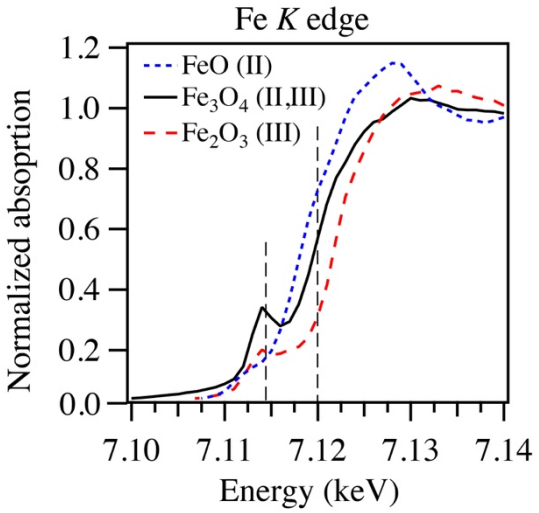

Fig. 2: Fe *K* XANES spectra of Fe_3O_4, FeO, and Fe_2O_3. After Ref. [3].

In this experiment, we carried out usual XFH measurements at room temperature with 21 incident x-ray energies, E_0, from 7.5 to 17.5 keV in steps of 0.5 eV to obtain averaged atomic images around the Fe ions. After then, the measurements were performed at E_0 = 7.114 and 7.120 keV, where the Fe^{3+} and Fe^{2+} contributions are emphasized for the central atoms, respectively. A similar experiment was previously carried out by Ang *et al.* [3]. They, however, chose different E_0 = 7.125 and 7.130 keV, where the contrasts between the Fe^{2+} and Fe^{3+} ions were not clearly detected.

A single crystal Fe_3O_4 magnetite was purchased from SurfaceNet GmbH through an agency Crystal Base Co., Ltd. having a flat (001) surface with an area of 5 × 5 mm^2. Figure 3 shows a schematic top view of the XFH apparatus used for the present experiments. Fe $K\alpha$ XFH measurements were carried out at BL6C of the PF-KEK. The sample was placed on a rotatable table. The incident x-rays with a size of 0.3 × 0.3 mm^2 were focused onto the (001) surface of the sample. The measurement was performed in inverse mode [5] by changing the incident angle $0° \leq \theta \leq 75°$ in steps of 1° and the azimuthal angle $0° \leq \phi \leq 360°$ in steps of 0.35°. The Fe $K\alpha$ fluorescent x-rays with an energy of 6.403 keV were collected by using an avalanche photodiode (APD) detector *via* a toroidal graphite crystal energy analyzer. The experimental details are given in review papers [5,6].

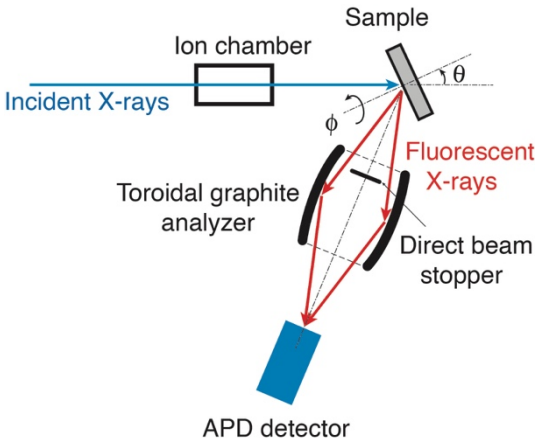

Fig. 3: Schematic top view of XFH apparatus.

Holograms were evaluated by firstly normalizing experimental fluorescent x-ray intensities to the incident x-ray ones monitored with an ion chamber, and secondly by subtracting the geometrical background of the sample. Extensions to the holographic data to the full solid angles were carried out by using the measured x-ray standing wave (XSW) curves in the holograms.

We employed an analytical method of a "scattering pattern matrix extraction algorithm using an L_1 regularized linear regression" (SPEA-L1) designed by Matsushita [7], which is based on an inverse problem and represents a sparse modeling approach. Details of this analytical procedure are given in Ref. [7], and its feasibility is described by applying it to several examples [8].

3 Results and Discussion

Figure 4 exhibits the Fe $K\alpha$ holograms measured at E_0 = 11.5 keV, which is drawn under an orthographic projection. θ and ϕ are respectively given by the radial and angular directions of the figure. A roughly fourfold symmetry including sharp XSW signals was observed in the holographic pattern, indicating a good quality of the single crystal.

Figure 5 represents the averaged atomic images around the Fe atoms on the (001) plane at z = 0 nm obtained by 21 holograms measured at E_0 = 7.5 – 17.5 keV. In this plane, only the Fe atoms are located. Due to the very large number of the holograms compared with usual previous experiments, the atomic images are clearly obtained with an extremely low artifact level.

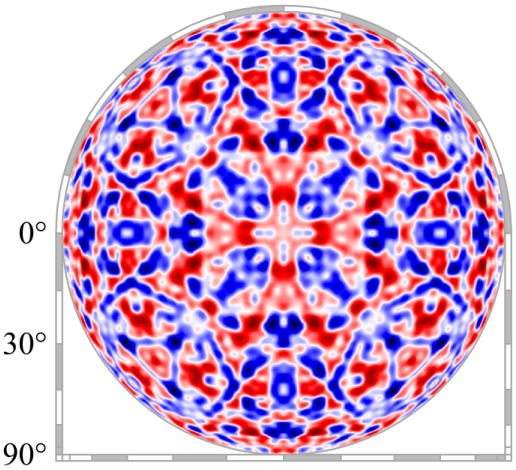

Fig. 4: XFH hologram measured at E_0 = 11.5 keV.

Note that intense images are seen in the ideal positions around the A site, while those around the B sites are relatively weak. This would be due to the coexistence of different valent Fe ions. Namely, the A sites are occupied by only Fe^{3+} ions, and thus, the local environments around the A sites are rather simple, causing the intense atomic image intensities at the ideal positions around the A sites. On the other hand, both the Fe^{2+} and Fe^{3+} ions with different ionic radii enter the B sites. Therefore, positional fluctuations would be caused in the positions of neighboring atoms around the B sites.

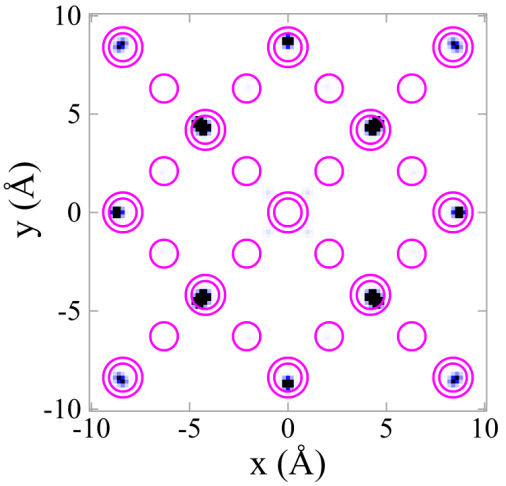

Fig. 5: Atomic images on the (001) plane at z = 0. Large and small circles indicate the ideal Fe atomic positions around the Fe atoms at the A and B sites, respectively.

Figure 6 shows atomic images around the Fe atoms on the (001) plane at z = 0 nm obtained at E_0 = (a) 7.114 and (b) 7.120 keV, which are taken from Ref. [6]. The magnitudes of the images are normalized to that of the strongest ones, and indicated as the gray scale bar beside the figures.

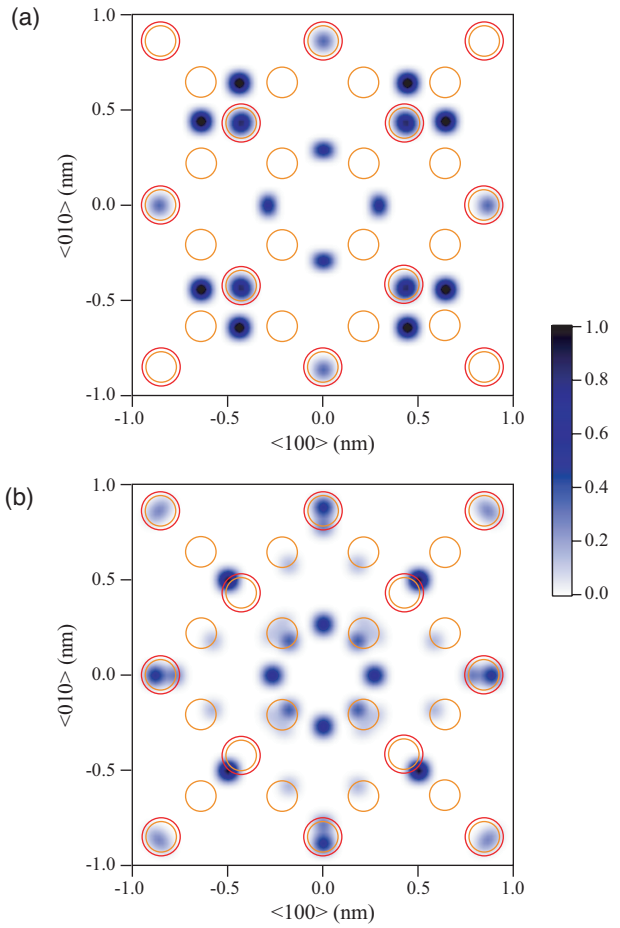

Fig. 6: Atomic images around the Fe atoms on the (001) plane at z = 0 nm obtained at E_0 = (a) 7.114 and (b) 7.120 keV. After Ref. [6].

In (a), the Fe^{3+} ions dominate the atomic images. Although strong artifacts are seen outside of the ideal positions, the most intense atomic images are observed at the ideal positions of the tetrahedral A sites, which looks similar to the averaged atomic images shown in Fig. 5.

In (b), on the other hand, the Fe^{2+} ions largely contribute the atomic images. The obtained atomic images are weak and show features different from those in (a). Firstly, images are observed near the ideal positions of both the A and B sites, which are expected by diffraction experiments. Secondly, the positions are slightly shifted from the ideal ones, and thus, large lattice distortions are expected around the Fe^{2+} ions.

Summary

Valence-selective XFH experiments were performed on an Fe_3O_4 mixed valence magnetite crystal, and clear signs of differences were observed in the lattice distortions around the Fe^{2+} and Fe^{3+} central ions. Based on the present experimental results, extents of the lattice distortions will be clarified by comparing with theoretical calculations, which was succeeded in our previous literatures [9].

Acknowledgement

The XFH experiments were performed at BL6C of the PF-KEK (No. 2019G635). This work was supported by the Japan Society for the Promotion of Science (JSPS) Grant-in-Aid for Innovative Areas '3D Active-Site Science' (Nos. 26105006 and 26105013) and 'Sparse Modeling' (No. 16H01553), and for Transformative Research Areas (A) 'Hyper-ordered structures' (No. 20H05878), the Japan Science and Technology Agency (JST) CREST (No. JPMJCR1861), and the Deutsche Forschungsgemeinschaft (DFG) Mercator Fellowship in FOR 2824.

References

[1] S. Hosokawa *et al., J. Phys. Soc. Jpn.* **89**, 034603 (2020).
[2] L. W. Finger *et al.*, *Phys. Chem. Minerals* **13**, 215 (1986).
[3] A. K. R. Ang *et al.*, *Phys. Status Solidi B* **255**, 1800100 (2018).
[4] R. D. Shannon. *Acta Crystallogr.* **A32**. 751 (1976).
[5] K. Hayashi *et al.*, *J. Phys.: Condens. Matter* **24**, 093201 (2012).
[6] S. Hosokawa *et al., Jpn. J. Appl. Phys.* **58**, 120601 (2019).
[7] T. Matsushita, *e-J. Surf. Sci. Nanotech*. **14**, 158 (2016).
[8] S. Hosokawa *et al.*, *Phys. Status Solidi B* **255**, 1800089 (2018).
[9] S. Hosokawa *et al., Phys. Rev. B* **87**, 094104 (2013).

* shhosokawa@kumamoto-u.ac.jp